The Conformational Dynamics of a Metastable Serpin Studied by Hydrogen Exchange and Mass Spectrometry

ARTICLE *in* BIOCHEMISTRY · JUNE 2006

Impact Factor: 3.02 · DOI: 10.1021/bi060431f · Source: PubMed

4 AUTHORS, INCLUDING:

Patrick L Wintrode
University of Maryland, Baltimore
54 PUBLICATIONS **1,586** CITATIONS

SEE PROFILE

Articles

The Conformational Dynamics of a Metastable Serpin Studied by Hydrogen Exchange and Mass Spectrometry

Yuko Tsutsui,[‡] Lu Liu,[§] Anne Gershenson,[§] and Patrick L. Wintrode*[,‡]

Department of Physiology and Biophysics, Case Western Reserve University, Cleveland, Ohio 44106, and Department of Chemistry, Brandeis University, Waltham, Massachusetts 02454

Received March 3, 2006; Revised Manuscript Received April 6, 2006

ABSTRACT: Serpins are a class of protease inhibitors that initially fold to a metastable structure and subsequently undergo a large conformational change to a stable structure when they inhibit their target proteases. How serpins are able to achieve this remarkable conformational rearrangement is still not understood. To address the question of how the dynamic properties of the metastable form may facilitate the conformational change, hydrogen/deuterium exchange and mass spectrometry were employed to probe the conformational dynamics of the serpin human α_1-antitrypsin (α_1AT). It was found that the F helix, which in the crystal structure appears to physically block the conformational change, is highly dynamic in the metastable form. In particular, the C-terminal half of the F helix appears to spend a substantial fraction of time in a partially unfolded state. In contrast, β-strands 3A and 5A, which must separate to accommodate insertion of the reactive center loop (RCL), are not conformationally flexible in the metastable state but are rigid and stable. The conformational lability required for loop insertion must therefore be triggered during the inhibition reaction. β-strand 1C, which anchors the distal end of the RCL and thus prevents transition to the so-called latent form, is also stable, consistent with the observation that α_1AT does not spontaneously adopt the latent form. A surprising degree of flexibility is seen in β-strand 6A, and it is speculated that this flexibility may deter the formation of edge−edge polymers.

Inhibitory serpins act through a unique mechanism (*1*). Unlike other protease inhibitors, which simply bind to the active sites of their targets, serpins structurally disrupt their target proteases, trapping the acyl−enzyme intermediate. This disruption is accomplished through a massive conformational change in the serpin molecule (*2*−*4*). During cleavage of the reactive center loop (RCL)[1] by a target protease, a covalent bond is formed between the protease and serpin. This covalent bond is kept intact while the RCL translocates to the opposite end of the serpin structure and inserts into the middle of the central A β sheet (parts a and b of Figure 1), becoming a sixth strand. As a result of this covalent bond, the bound protease is translocated along with the RCL. Transolcation of the protease relative to the serpin and the resulting force on the ester bond pulls the catalytic Ser 6 Å out of the protease active site, resulting in inhibition (*2*, *4*). As a result of loop insertion, the serpin becomes substantially more stable (active serpins unfold at ∼60 °C, while cleaved serpins unfold at ≥120 °C) (*5*). It has been proposed that the inhibitory active form of the serpin structure is destabilized by conformational strain, resulting from poor packing of residues (including steric clashes and cavities) (*6*−*9*). Structural analysis of the cleaved form shows that packing is improved in this conformation, and the cleaved form is thus sometimes referred to as the "relaxed" form (*10*). Even in the absence of cleavage by a protease, the RCL can insert into β-sheet A, resulting in a "latent" conformation that is also more stable than the active form (*1*). These observations indicate that serpins, unlike most other proteins, do not initially fold to their global free-energy minimum but instead adopt a metastable conformation, and this metastability is intimately linked to their biological function.

The major structural features of the highly conserved serpin fold are illustrated in Figure 1c with the canonical serpin α_1-antitrypsin (α_1AT) (*6*). α_1AT consists of nine α helices (labeled A−I) and three β sheets (A, B, and C). In the cleaved and latent forms, the RCL inserts between strands three and five of β-sheet A. Studies have identified several regions that are important for the native → cleaved and native → latent transitions (*10*, *11*). The highly conserved "breach" region is located at the top of β-sheet A and is the site of initial RCL insertion. The "shutter" region, which is also highly conserved, includes the middle of strands 3A and 5A, as well as a portion of strand 5B, and is believed to control the opening of β-sheet A (*10*, *11*).

* To whom correspondence should be addressed: Department of Physiology and Biophysics, Case Western Reserve University, Cleveland, OH 44106. Telephone: (216) 368-3178. Fax: (216) 368-3952. E-mail: patrick.wintrode@case.edu.

[‡] Case Western Reserve University.

[§] Brandeis University.

[1] Abbreviations: α_1AT, α_1-antitrypsin; RCL, reactive center loop; H/D-MS, hydrogen exchange mass spectrometry.

10.1021/bi060431f CCC: $33.50
Published on Web 05/06/2006

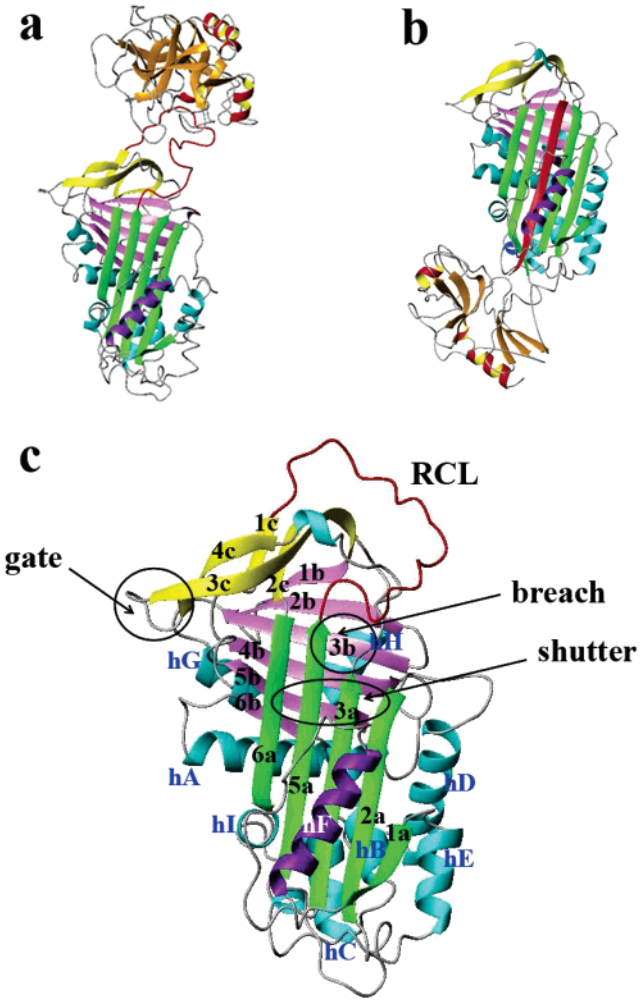

FIGURE 1: (a and b) Conformational transition during inhibition. (a) Encounter complex between a serpin and target protease (PDB ID 1K9O) (*3*). The protease is shown in orange. (b) Inhibitory complex of a serpin and translocated protease (PDB ID 1EZX) (*2*). The inserted RCL is shown in red. The F helix is shown in purple. (c) Structure of active α_1AT (PDB ID 1QLP) (*6*). Functionally important regions as described by Whisstock et al. are indicated in circles. β-Sheets A, B, and C are in green, pink, and yellow, respectively. All α helices are shown in cyan. The RCL is shown in red. All figures were prepared with MOLMOL (*38*).

The structures of numerous serpins in a variety of different conformations have been solved by X-ray crystallography (*1*). In addition, for α_1AT, extensive mutagenesis studies have identified amino acid substitutions affecting stability and/or inhibitory activity (*9*). Little is known, however, about the dynamics of serpins in their inhibitory active conformation. What is the distribution of rigidity and flexibility in the active serpin molecule? Is there a relationship between the conformational motions of serpins in the active state and the motions that they must undergo during the transition to the cleaved form? Several regions in the serpin structure must experience large displacements during the active → cleaved transition; are these same regions already flexible even before the RCL is cleaved? Answers to these questions would shed light on the relationship between serpin structure and function.

Hydrogen/deuterium (H/D) exchange is a powerful method for probing the conformational dynamics of proteins in solution (*12*, *13*). Backbone amide hydrogens can exchange with deuterium when a protein is incubated in D_2O. Amide hydrogens that are not involved in hydrogen bonding and located on the protein surface or in unstructured regions will exchange rapidly, typically within several seconds at neutral pH. If an amide hydrogen is buried in the protein interior or participates in hydrogen bonding, it will exchange only when fluctuations occur that disrupt its interactions with neighboring groups and expose it to the solvent. The exchange process may be described by the model (*12*, *13*)

$$\text{closed(H)} \underset{k_{close}}{\overset{k_{open}}{\rightleftharpoons}} \text{open(H)} \xrightarrow{k_{int}} \text{open(D)} \underset{k_{open}}{\overset{k_{close}}{\rightleftharpoons}} \text{closed(D)}$$

where closed and open represent conformations in which amide hydrogen atoms are inaccessible or accessible to the solvent, respectively. The observed rate constant for the exchange (k_{obs}) is expressed as

$$k_{obs} = \frac{k_{open}k_{int}}{k_{close} + k_{int}} \quad (1)$$

where k_{open} and k_{close} are rate constants for opening and closing processes, respectively, and the intrinsic exchange rate constant (k_{int}) is the exchange rate constant for a completely unprotected amide hydrogen. At neutral pH and in the absence of denaturants, $k_{close} \gg k_{int}$ so that eq 1 simplifies to

$$k_{obs} = \frac{k_{open}k_{int}}{k_{close}} = K_{eq}k_{int} \quad (2)$$

Thus, the degree to which a protein structure is susceptible to transient disruptions by conformational fluctuations is reflected in the exchange rates of amide hydrogens with deuterium.

In this study, H/D exchange measured by mass spectrometry was employed to monitor the conformational dynamics of the 44 kD serpin WT-α_1AT in its active conformation, providing a detailed view of the distribution of conformational flexibility in this metastable protein. Further, knowledge of this distribution reveals whether functionally important regions in the structure are particularly flexible or rigid, providing an additional link between structure and function.

MATERIALS AND METHODS

Expression, Purification, and Activity of Wild-Type (WT-α_1AT). WT-α_1AT was expressed and purified on the basis of the method of Kwon et al. (*14*) with slight modifications. WT-α_1AT was expressed as a recombinant protein in *Escherichia coli* BL21 (DE3) cells carrying pEAT8-137 plasmid (*15*). All chemicals were obtained from Sigma unless otherwise specified. Cells were cultured at 37 °C, followed by induction with 1 mM isopropyl β-D-1-thiogalactopyranoside. Cells were lysed in 50 mM Tris-HCl (pH 8.0), 50 mM NaCl, 1 mM ethylenediaminetetraacetic acid (EDTA), 1 mM phenylmethanesulfonyl fluoride (PMSF, Roche), 1 mM β-marcaptoethanol (Bio-Rad) (buffer A) containing 0.2 mg/mL of lysozyme followed by sonication with a 6 × 30 s cycle. Cells were centrifuged at 14 000 rpm for 45 min to isolate inclusion bodies. Inclusion bodies were washed twice with buffer A containing 0.5% Triton X-100 (Fluka). The inclusion bodies were dissolved in buffer A containing 8 M

urea and refolded into 1.5 L of 10 mM sodium phosphate (pH 6.5), 1 mM EDTA, 0.2 mM PMSF, and 1 mM β-marcaptoethanol (buffer B). The sample was incubated at 25 °C for 1 h to refold and loaded onto Hiprep 16/10 DEAE FF (Amersham). Proteins were eluted with a linear gradient of 200 mL of buffer B containing 1 M NaCl. Fractions containing α_1AT were pooled, and the fractions were buffer-exchanged into 20 mM bistris (pH 6.5), 1 mM EDTA, and 1 mM β-marcaptoethanol (buffer C) with Amicon Ultra-15 (Millipore) and Microcon YM-30 (Millipore). The sample was loaded onto MonoQ 4.6/100 PE (Amersham), and α_1-AT was eluted with a linear gradient of 30 mL of buffer C containing 250 mM NaCl. Fractions containing α_1AT were pooled and buffer-exchanged into 10 mM sodium phosphate (pH 7.8) and 50 mM NaCl. The concentration of α_1AT was determined in 6 M guanidine chloride using $A_{1cm}^{1\%} = 4.3$ at 280 nm as described previously (*7*).

The active concentration of bovine trypsin (Sigma) was determined as described previously using *P*-nitrophenyl-*P*′-guanidino-benzoate (Sigma) as a substrate (*16*). The stoichiometry of inhibition (SI), the ratio of moles of α_1AT required to inhibit 1 mol of active trypsin, was determined as described previously (*17*). To determine the active concentration of α_1AT, different molar ratios of α_1AT and bovine trypsin were incubated in 10 mM sodium phosphate (pH 7.8) and 50 mM NaCl for 15 min at 25 °C with the trypsin concentration fixed. After the incubation, the sample was diluted 10-fold with 10 mM sodium phosphate (pH 7.8) and 50 mM NaCl to stop the reaction. The residual trypsin activity was determined by observing the absorption of hydrolysis product of N_α-benzoyl-L-arginine-4-nitroanilide hydrochloride (Sigma) at 410 nm. For all samples, the SI was determined to be 1.0, 100% active WT-α_1AT.

Peptide Mapping by High-Performance Liquid Chromatography (HPLC)−Tandem Mass Spectrometry. A total of 5 μg (0.1 nmol) of purified active α_1AT in 100 μL of 10 mM sodium phosphate (pH 7.8) and 50 mM NaCl was mixed with 95 μL of 100 mM NaH_2PO_4 (pH 2.4) followed by the addition of 5 μg of porcine pepsin dissolved in 0.05% TFA and H_2O for pepsin digestion. α_1AT was digested for 5 min on ice. The final concentration of α_1AT was 565 nM. The digested sample was injected into a micropeptide trap (Michrom Bioresources) connected to a C18 HPLC column (5 cm × 1 mm, Alltech) coupled to a Finnigan LCQ quadrupole ion-trap mass spectrometer (ThermoElectron). Peptic fragments were eluted using a gradient of acetonitrile (Burdick and Jackson) at a flow rate of 50 μL/min for a tandem mass spectrometry experiment to sequence each peptic fragment. Peptic fragments were identified by using the search algorithm SEQUEST (ThermoElectron) and manual inspection.

H/D Exchange. A sample containing 5 μg (0.1 nmol) of active WT-α_1AT in 10 mM sodium phosphate (pH 7.8) and 50 mM NaCl was diluted 24-fold with 10 mM sodium phosphate (pD 7.8) and 50 mM NaCl dissolved in D_2O at 25 °C (Cambridge Isotope Laboratories) to label the sample. The deuteration reaction was quenched at different time points by adding equal volume of 100 mM NaH_2PO_4 (pH 2.4) and quickly frozen in a dry ice−ethanol bath. Samples were stored at −80 °C until use. The final concentration of WT-α_1AT was 565 nM. All deuterated samples were made immediately after confirming 100% WT-α_1AT activity by the SI determination assay described above.

Isotope Analysis by HPLC−Electrospray Ionization Mass Spectrometry (ESIMS). The frozen sample was quickly thawed and digested with 5 μg of pepsin on ice for 5 min followed by immediate injection into a micropeptide trap connected to a C18 HPLC column coupled to a Finnigan LCQ quadrupole ion-trap mass spectrometer. Peptic peptides were eluted in 12 min using a gradient of 10−45% acetonitrile at a flow rate of 50 μL/min. The micropeptide trap and C18 HPLC column were immersed in ice to minimize back exchange.

Because the mass of a peptic fragment increases by one for every amide hydrogen atom exchanged with deuterium, the amount of deuterium in each peptic fragment can be determined by comparing the mass of a labeled peptic fragment with the mass of the same peptide without the label. The centroid mass of each peptic fragment was determined using the software package MagTran. To correct for the back-exchange reaction of hydrogen atoms during pepsin digestion and HPLC−MS, a fully deuterated sample was prepared by incubating 5 μg of α_1AT in 6 M guanidine deuterochloride, 10 mM sodium phosphate (pD 7.8), and 50 mM NaCl for 30 min at 25 °C. The deuterium incorporation of each peptic fragment, corrected for the back exchange, was calculated using the following equation (*12*, *13*):

$$D = \frac{m - m_{0\%}}{m - m_{100\%}} \times N \quad (3)$$

where m is the mass of deuterated peptic fragment, $m_{0\%}$ and $m_{100\%}$ are the mass of the unlabeled and fully deuterated peptic fragments, respectively, N is the total number of exchangeable amide hydrogen atoms in each peptic fragment, and D is the number of amide hydrogen atoms incorporated in each peptic fragment. The number of deuterium, D, in each peptic fragment was plotted versus time and fitted to the following equation:

$$D = N - N_{fast}e^{-k_{fast}t} - N_{int}e^{-k_{int}t} - N_{slow}e^{-k_{slow}t} \quad (4)$$

where N_{fast}, N_{int}, and N_{slow} are the number of fast-, intermediate-, and slow-exchanging amide hydrogen atoms, respectively. The corresponding observed exchange rate constants are k_{fast}, k_{int}, and k_{slow}. Nonlinear least-squares fitting was carried out using ORIGIN (OriginLab).

RESULTS

Peptide Mapping and Coverage. Tandem mass spectrometry experiments identified 94 peptic fragments covering 92% of the α_1AT sequence. The rapid HPLC gradient employed for hydrogen exchange mass spectrometry (H/D-MS) experiments reduced the sequence coverage to 89%. The 29 peptic fragments analyzed in H/D-MS experiments are well-distributed throughout the molecule, and the only significant gap consists of β-strand 2A (Figure 2).

H/D Exchange. H/D exchange of active α_1AT was performed at pD 7.8 at 25 °C followed by HPLC−MS to quantify the mass of each peptic fragment. Figure 3 shows normalized deuterium uptake as a function of time mapped onto the sequence of α_1AT. In general, regions containing significant α-helical or β-sheet content exchange more slowly

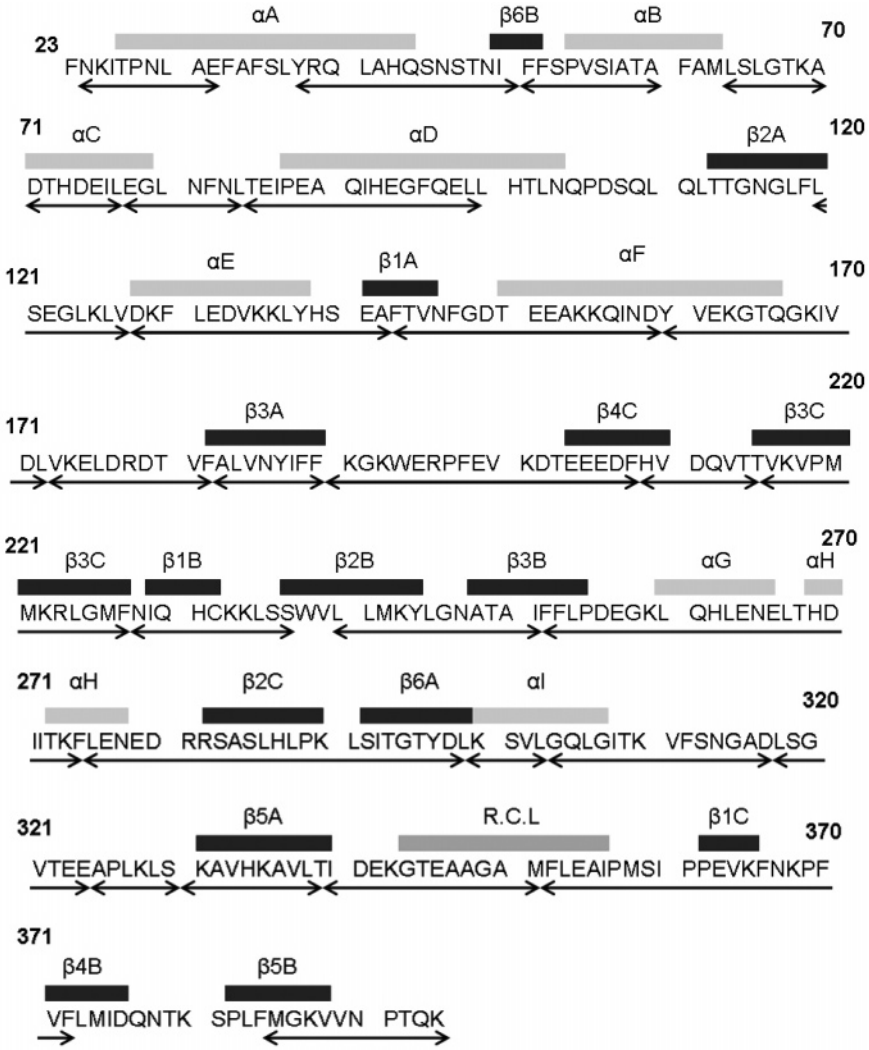

FIGURE 2: Peptic fragments used for H/D exchange analysis. Peptic fragments are indicated by double-headed arrows under the sequence of α_1AT. Some overlapping fragments have been omitted for clarity. Amino acid sequences corresponding to either α helices or β strands are shown below light gray or black bars, respectively. The RCL is also shown below a gray bar.

than regions composed chiefly of loops or turns. For example, it is clear that residues 51−78 (containing helices B and C), 215−245 (containing strands 3C, 1B, and 2B), and particularly 331−340 (strand 5A) show slow exchange. Additionally, the peptide consisting entirely of β-strand 3A (183−190) clearly exchanges more slowly then either of the two peptides flanking it, which are largely without secondary structure. Surface loops such as the RCL, in contrast, show rapid exchange. There are, however, some exceptions to this trend. Residues 160−171 include six residues in the C-terminal region of the F helix, yet this peptide exchanges at a rate similar to that observed for unstructured surface loops such as the RCL. Similarly, residues 276−299 show rapid exchange despite the fact that they include all of β-strands 2C and 6A. The loop region between helix I and strand 5A shows a somewhat slower exchange then other loops in the protein, and this reflects the lack of solvent-accessible backbone amides seen in this region in the X-ray crystal structure.

From the mass shift of the peptide isotopic envelopes over time (Figure 4a), deuterium incorporation was calculated and deuterium versus time curves were each fit to a sum of three exponentials as described in the Materials and Methods. Normalized deuterium versus time curves for two typical peptides (160−171 and 325−338), along with best fits, are shown in Figure 4b. Exchange rate constants and the number of fast-, intermediate-, and slow-exchanging amide hydrogens in each peptic fragment are given in Table 1. The rate constants for fast-exchanging hydrogens are on the same order of magnitude as exchange rate constants found in unstructured peptides (*18*). Thus, the obtained fast exchange rate constants most likely represent exchange rate constants for amide hydrogen atoms that are fully solvent-exposed. Half-lives for intermediate-exchanging hydrogens range from 30 s to ~15 min. These rates are generally much slower than those of completely unprotected hydrogens but are still considerably faster than rates observed for hydrogens in stable regions of folded proteins. These hydrogens likely are in regions that are structured but are marginally stable and undergo frequent fluctuations. Half-lives for slow-exchanging hydrogens range from 488 s for peptide 24−32 to 1.7×10^6 s for peptide 190−208, indicating that these peptides are derived from regions that are both structured and stable. It must be noted that the reported rate constants for slow hydrogens are limited by our longest exchange time and thus represent upper limits for the true rate constants.

One drawback of H/D-MS is that it is not generally possible to achieve single-residue resolution. Because peptic

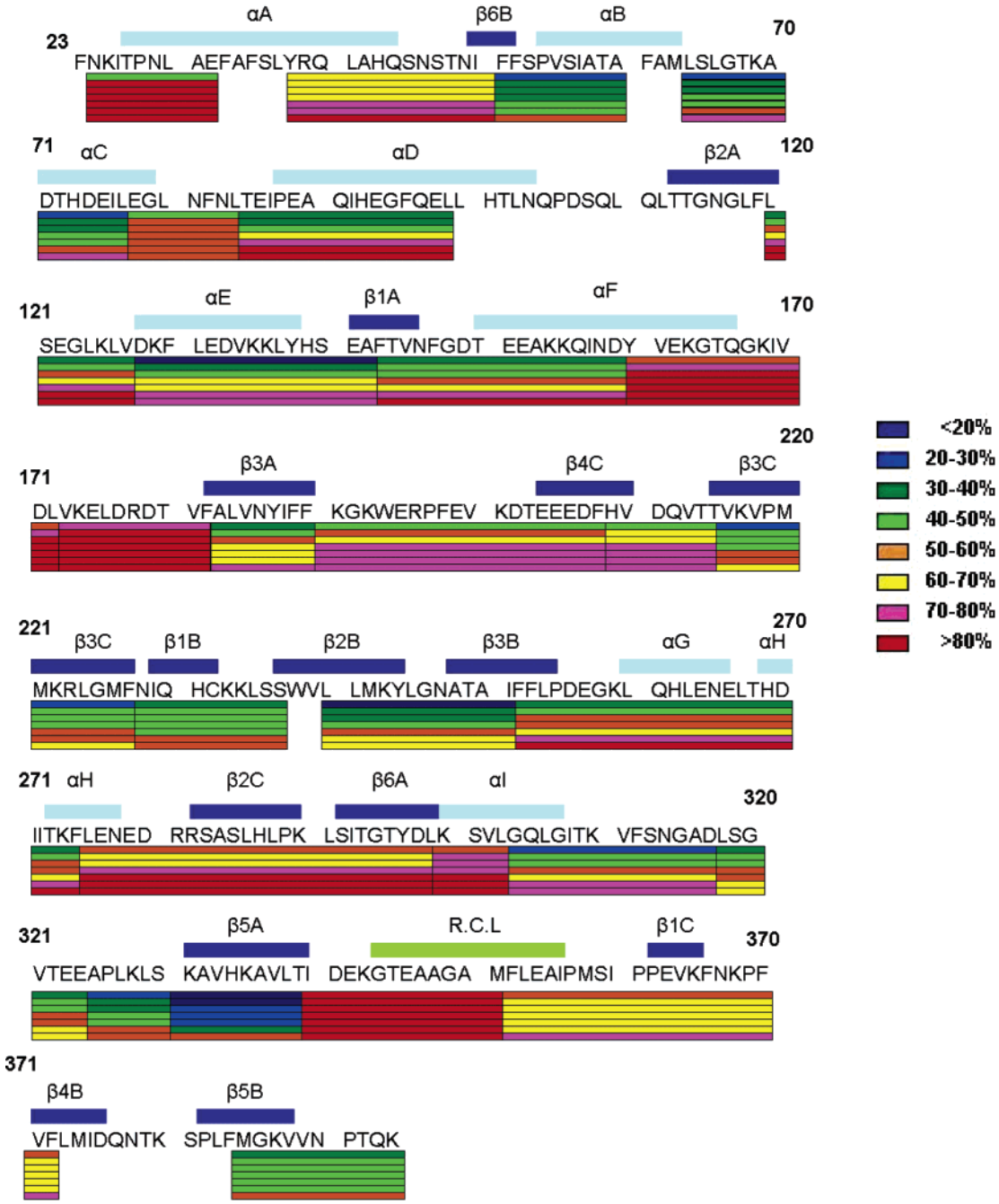

FIGURE 3: Percent exchange of peptides derived from different regions of α_1AT. Colored bars below the sequence represent, in descending order, deuterium uptake at 10, 50, 100, 500, 1000, 2000, and 3000 s. Regions corresponding to α helices or β strands are shown in light blue or dark blue bars, respectively. The RCL (344−356) region is shown below a light green bar.

fragments, especially the longer ones, may include multiple structural regions when mapped onto the crystal structure of the intact protein, simply ranking peptides by the exchange rate may be misleading. For example, if a particular peptide is derived from a region that is $^1/_4$ β-strand and $^3/_4$ surface-exposed loop, the peptide as a whole will display rapid exchange even if the β strand itself is stable. To address this, we adopt the following procedure: for each peptide, we first count the number of amide hydrogens that are hydrogen-bonded as part of an α helix or β sheet [by analyzing the crystallographic structure using WhatIf (*19*)]. These hydrogens should exchange slowly if the secondary structures are stable. We then compare this number with the number of slow hydrogens that are experimentally observed for that same peptide. For example, if a peptide contains 10 amide hydrogens in an α helix but only 3 slow-exchanging hydrogens are observed, this indicates that a significant portion of the α helix must be highly flexible. This method has the virtue that it will not overestimate the degree of flexibility in these secondary structures, although it can underestimate it (if the assumption that the slow hydrogens are located in helices and sheets is incorrect, this merely implies that these structures are even more flexible). In Figure 5, the α helices and β strands of α_1AT are color-coded according to the method just described: where the number of expected and observed slow-exchanging hydrogens is in good correspondence (observed/expected ratio > 80%), the structure is colored blue, and where there is a large

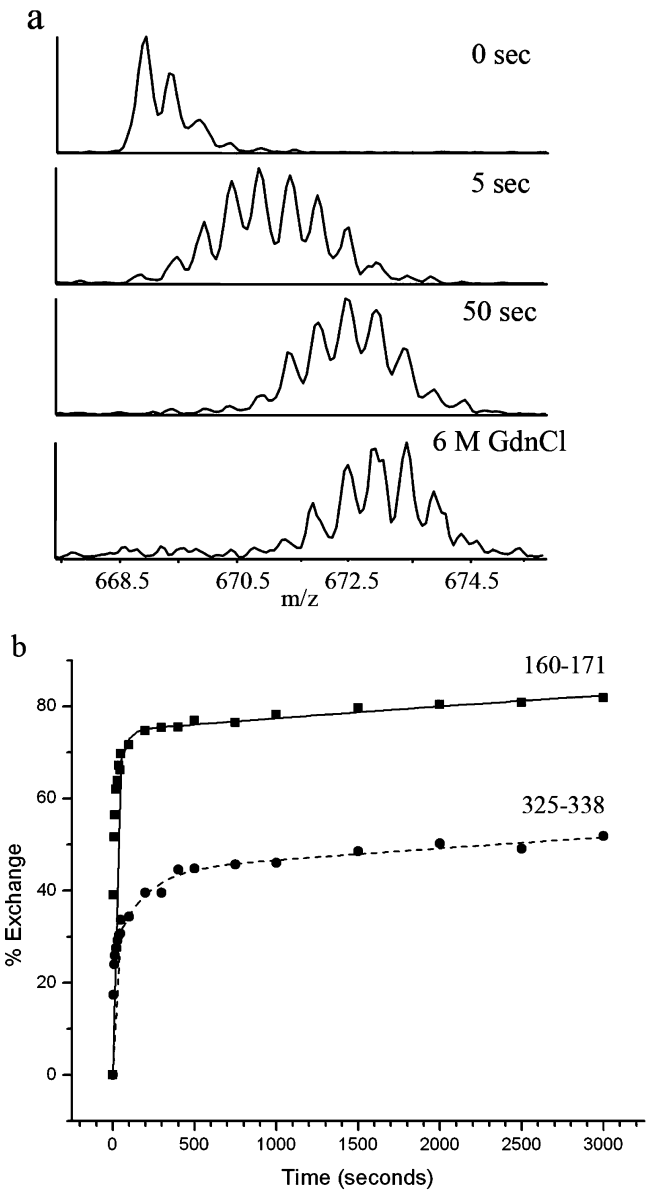

FIGURE 4: (a) MS spectra of doubly charged peptide 160−171. Deuterium uptake of the peptide 160−171 at 0 (nondeuterated reference), 5, 50 s and in 6 M guanidine deuterochloride (fully deuterated reference) is shown. (b) Normalized deuterium uptake versus time curves for two peptic fragments derived from α_1AT. Peptides are 160−171 (■, —) and 325−338 (●, - - -). Lines represent the best fit to eq 4.

discrepancy (ratio <20%), it is colored red, with a scale of intermediate colors. This presentation of the H/D exchange data complements the whole peptide exchange behavior presented in Figure 3. The two methods of visualizing the H/D exchange results are generally in agreement regarding flexible and rigid regions (e.g., that rigidity of β-sheet B and the flexibility of helix F). There are, however, some differences. β-strands 1C, 2C, and 4C are all contained in peptic fragments that also contain substantial amounts of surface-exposed loop. On the basis of the exchange behavior of whole peptides, these β-strands appear to be flexible, but when the numbers of solvent-exposed versus hydrogen-bonded amide hydrogens in each peptide are taken into account, as just described, these same strands appear to be stable. For example, residues 352−372 include six hydrogen-bonded amide hydrogens according to the crystal structure, three in β-strand 1C and three in β-strand 4B, while the remaining eleven amide hydrogens are in exposed loops. Experimental H/D exchange results for peptide 352−372 indicate six slow-exchanging hydrogens, strongly suggesting that the hydrogen bonds in strands 1C and 4B are stable.

Table 1: Results of Fitting H/D Exchange Curves to Eq 4

residues	N_{fast}	k_{fast} (s^{-1})	N_{int}	k_{int} (s^{-1})	N_{slow}	k_{slow} ($\times 10^{-5}$ s^{-1})
24−32	3	0.23	3	0.033	1	0.14
38−51	8	0.69	2	0.0020	3	3
38−60	6	0.40	3	0.0014	12	1
64−77	4	0.44	3	0.0026	6	3
64−84	10	0.42	1	8×10^{-4}	9	0.4
85−99	4	0.35	5	0.0038	4	2
120−142	8	0.36	7	0.0051	7	2
127−142	3	0.16	7	0.0033	5	7
131−142	3	0.085	4	0.0041	3	2
143−159	6	0.38	6	0.0014	4	3
160−171	7	0.17	2	0.0059	2	2
160−172	9	0.12	2	0.0038	1	0.9
173−182	6	0.69	2	0.024	1	0.23
183−208	9	0.29	6	0.0068	9	2
190−208	8	0.27	5	0.0035	4	0.04
209−227	7	0.23	2	0.0031	8	3
228−237	3	0.54	2	0.020	4	2
241−251	3	0.27	2	0.0015	4	0.9
251−275	9	0.23	6	0.0022	8	3
276−299	14	0.29	6	0.0019	2	7
297−303	3	0.37	1	0.0031	2	5
304−317	5	0.21	5	0.0019	4	1
318−338	7	0.20	4	0.0082	8	1
325−338	3	0.17	3	0.0031	6	0.6
339−351	10	1.0	1	0.0015	1	5
352−372	9	0.39	1	0.039	6	2
385−394	3	0.63	1	0.0044	4	0.6

DISCUSSION

Previous structural and mutagenesis studies have shown that α_1AT in the active state is strained because of overpacking of buried residues, as well as a large number of cavities and surface pockets (*7*−*9*). Although mutations that ameliorate the strain, such as those that fill cavities, can increase the stability of α_1AT in the active state, these mutants have decreased inhibitory activity (*7*−*9*). This tradeoff between stability and function implies that the metastability of α_1AT in the active state is important for function and that local instabilities distributed throughout active α_1AT may play a critical role in achieving the large conformational change required for protease inhibition.

In this study, the distribution of local conformational flexibility in active α_1AT was probed by H/D-MS. The slow-exchanging core is composed of helices B and C, β-sheet B, and central strands of β-sheet A (Figure 5). This core region composed of conserved residues corresponds to the breach and shutter regions, previously suggested to play important roles in the active → cleaved conformational transition (*10*, *11*). For the RCL to insert into β sheet A, strands 3A and 5A must separate from each other. If the hydrogen bonds between these two strands were already labile in the active state, this would ease the transition to the cleaved form by lowering the energy barrier to loop insertion. In fact, the slow exchange observed in this region indicates that the amide hydrogen bonds between strands 3A and 5A are stable in the active form. Thus, the mobility that is required of this region during inhibition must be triggered by conformational rearrangements that occur after RCL

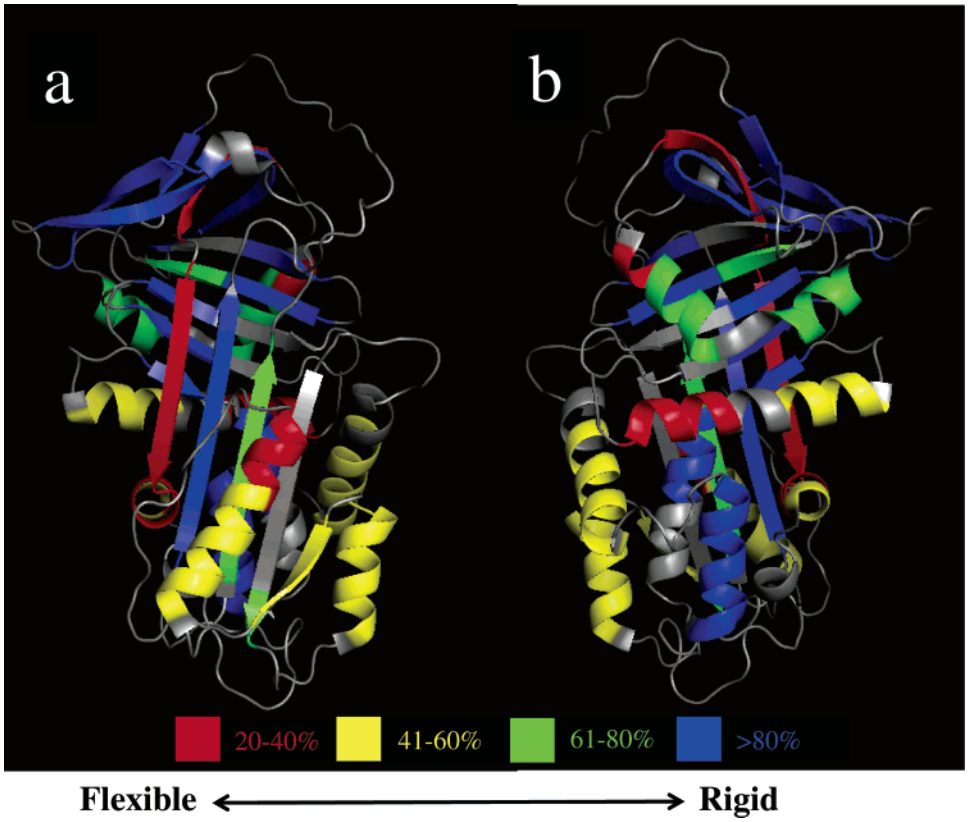

FIGURE 5: Three-dimensional structure of active α_1AT (PDB ID 1QLP) with α helices and β strands colored according to the ratio of the number of slow-exchanging hydrogens (experiment)/the number of protected hydrogens (determined from WhatIf) as described in the Results. (a) Front view of the structure of active α_1AT with stability color coded. The structure is rotated 180° about the *y* axis in b. Loops are colored gray in both figures. The figure was prepared with PyMOL (*39*).

cleavage. Im et al. (*20*) engineered α_1AT variants in which the RCL was extended by the insertion of $(GlyGlySer)_n$ repeats (where $n = 2$, 3, 5, or 10), and the stability of those folded mutants was found to be increased by up to 30 kcal/mol compared to the WT-α_1AT presumably because of folding to the more stable latent form. On the basis of these findings, they suggested that interactions between β-strands 3A and 5A in the active form are not sufficient to prevent loop insertion. However, our H/D exchange results do not indicate significant flexibility in β-strands 3A and 5A. Because Im et al.s' were refolding experiments, the degree of the active structure in β-sheet A at the time of loop insertion is unknown Thus, a direct comparison of the lability of strand 3A−5A interactions implied in the study of Im et al. with the rigidity seen in the present study cannot therefore be made.

Much of β-sheet C also exhibits slow exchange. Separation of β-strand 1C from the neighboring strand 2C is required for the transition to the latent form to occur (*21*−*23*). The peptide derived from strand 1C contains six residues that form hydrogen bonds as part of β strands (three from strand 1C and three from strand 4B), and our results indicate six slow-exchanging amide hydrogen atoms in this peptide with an average rate constant of 2×10^{-5} s^{-1}. Thus, the amide hydrogen bonds that fix strand 1C appear to be stable, in keeping with the fact that active WT-α_1AT does not spontaneously convert to the latent form. The stability of strand 1C together with the stability of strands 3A and 5A in active WT-α_1AT appears to prevent the latency transition.

Numerous α_1AT mutations have been identified in the human population, which result in misfolding and/or polymerization (*24*, *25*). These mutations can be categorized as (1) those which retard protein folding, (2) those which result in folding or conversion to the latent form, and (3) those which promote polymerization from the folded form. This latter class of mutations are believed to act by forcing the structure to expand and creating an opening between β-strands 3A and 5A, thus allowing the RCL of another molecule to insert and form a loop−sheet linkage (*10*). All but one (G115S) of the loop−sheet polymer-promoting mutations occur in the regions that we define as the slow-exchanging core of α_1AT. Likewise, mutations that result in spontaneous conversion to the latent form are also located in the slow-exchanging core (*24*). This is consistent with the observation that these mutations disrupt the active conformation of α_1AT (*24*). There is no similarly clear trend with regard to misfolding mutations. Glu342Lys and Asp256Val are both located in fast-exchanging loop regions, while Leu41Pro is located in a region of helix A, which shows reasonable protection against exchange.

In the available crystal structures of active and cleaved serpins, the F helix lies directly in the path that the RCL and bound protease must traverse during the conformational transition that results in inhibition (Figure 1a). The F helix must, therefore, be displaced during the active → cleaved transition and return to its position on the face of β-sheet A when the transition is complete. This could be accomplished either by a rigid-body movement of the F helix or by partial helix unfolding (*26*, *27*). The rate of H/D exchange observed in the C-terminal half of the F helix is comparable to exchange rates in solvent-exposed loops such as the RCL, indicating that this region is extremely labile in the active

state, possibly populating a partially unfolded conformation. Such conformational flexibility could ease the active → cleaved transition because a highly flexible and/or marginally stable F helix will be more readily displaced from its position at the front of β-sheet A. Several independent lines of evidence indicate that lability in the F helix plays a role in the active → cleaved transition. On the basis of site-directed mutagenesis experiments, it was suggested that the F helix undergoes conformational changes at both the N and C termini during inhibition (*26*). In another study, G117 in β-strand 2A was mutated to a series of residues with hydrophobic side chains capable of interacting with Y160 in the top of the F helix (*28*). These mutations, which fill a cavity, both stabilize the active state and decrease inhibitory activity without affecting the association rate constant with a target protease. Thus, flexibility at the top of the F helix is likely required for the translocation of target proteases. In a naturally occurring variant of the serpin antichymotrypsin, a conformation has been observed in which the last turn of the F helix is unraveled and it as well as the loop connecting it to strand 3A are inserted between strands 3A and 5A, forcing them apart (*29*). It has been proposed that this structure represents an intermediate state formed during inhibition, with the F helix facilitating loop insertion be parting strands 3A and 5A. All of these results suggest that pre-existing flexibility in the F helix, as observed here by H/D exchange, would facilitate the active → cleaved transition.

Surprisingly, a high degree of flexibility is observed in residues 276−299. This region encompasses a portion of the helix H and all of β-strands 2C and 6A, which should be well-ordered. There are 13 amide hydrogen atoms participating in hydrogen bonding in this region, yet H/D exchange result indicates only 2 slow-exchanging amide hydrogen atoms and 6 intermediate-exchanging amide hydrogen atoms in this region. This surprising flexibility may be explained by the functional requirement to avoid aggregation. β-Strand 6A is a largely solvent-exposed edge strand. Such edge β-strands present a potential danger because their conformation allows them to interact with any other edge strand that they encounter. Indeed, for the serpin plasminogen activator inhibitor I polymers have been crystallized in which the RCL of one molecule anneals to strand 6A of another, becoming strand 7A (*30*). A survey of known protein structures found that natural proteins employ a number of "negative design" strategies to suppress edge−edge interactions, including distortion from the optimal β-strand geometry and strategically placed prolines or charged side chains (*31*). The highly dynamic nature of β-strand 6A of α_1AT may represent an additional such strategy.

While little is known of the interactions of α_1AT with molecules other than its target proteases, several other serpins are known to participate in specific binding to other molecules for regulatory purposes. Antithrombin, heparin cofactor II, plasminogen activator inhibitor I, and protease nexin 1 are all known to interact with regulatory glycosaminoglycans, primarily through basic residues located in helix D (antithrombin residues near the adjacent N terminus of helix A are also involved) (*1*). Current theories of binding and allostery in proteins suggest that a pre-existing instability at a ligand-binding site is required for binding interactions to propagate to distant regions of a protein structure (*32*, *33*). H/D exchange indicates that both helix D and the N-terminal region of helix A are flexible (Figure 5). Of the nine hydrogen-bonded amides in helix D, only four are slow-exchanging, indicating that much of this helix experiences frequent conformational fluctuations. Although α_1AT does not require activation by glycosmainoglycan binding, the local flexibility in this region, if conserved, might be exploited by other serpins. Additionally, conformational lability in this region may be related to the evolution of the serpin family. Numerous evolutionary studies have suggested that conformationally flexible regions are more tolerant to mutations than rigid regions (*34*). Indeed, it is intriguing that the helix D completely lacks conserved residues among the serpin family (*11*). For example, in thermophilic bacteria such as *Pyrobaculum aerophilum* and *Thermobifida fusca*, helix D is absent or truncated respectively (*11*, *35*). Some viral serpins also lack helix D (*36*, *37*). However, these organisms are still capable of inhibiting target proteases, indicating that helix D does not directly participate in inhibition. Thus, during the course of the serpin evolution, residues in helix D were likely selected for functional regulation rather than for stability or inhibitory function.

CONCLUSIONS

This study has characterized the distribution of conformational flexibility in the canonical serpin human α_1AT and identified several features of potential functional significance. There has been much speculation on the role of the F helix in the serpin inhibitory mechanism because of its position in the structure where it apparently blocks the conformational change. Because the F helix must be somehow displaced from its position during the active → cleaved transition, the pre-existing flexibility in the F helix identified by H/D exchange may facilitate a rapid transition. Both the low degree of flexibility seen in β-strands 3A and 5A and the high flexibility in β-strand 6A may potentially discourage inappropriate conformational changes and/or polymerization, while the rigidity seen in β-strand 1C is consistent with its proposed importance in preventing the transition to the latent form. Numerous X-ray crystal structures of serpins in a variety of conformations are now available, but little is known regarding their conformational dynamics, despite the fact that dynamics may play an important role in serpin function. The present study of the serpin α_1AT is a first step toward filling in this missing piece of the current picture of serpin function.

ACKNOWLEDGMENT

We thank Dr. Frank Sönnichsen for helpful comments on our manuscript. This work is funded by Case Western Reserve University (to P. L. W.) and NSF Grant MCB-0446220 (to A. G.).

REFERENCES

1. Gettins, P. G. (2002) Serpin structure, mechanism, and function, *Chem. Rev. 102*, 4751−4804.
2. Huntington, J. A., Read, R. J., and Carrell, R. W. (2000) Structure of a serpin−protease complex shows inhibition by deformation, *Nature 407*, 923−926.
3. Ye, S., Cech, A. L., Belmares, R., Bergstrom, R. C., Tong, Y., Corey, D. R., Kanost, M. R., and Goldsmith, E. J. (2001) The

structure of a Michaelis serpin−protease complex, *Nat. Struct. Biol. 8*, 979−983.
4. Dementiev, A., Dobo, J., and Gettins, P. G. (2006) Active site distortion is sufficient for proteinase inhibition by serpins: Structure of the covalent complex of α_1-proteinase inhibitor with porcine pancreatic elastase, *J. Biol. Chem. 281*, 3452−3457.
5. Kaslik, G., Kardos, J., Szabo, E., Szilagyi, L., Zavodszky, P., Westler, W. M., Markley, J. L., and Graf, L. (1997) Effects of serpin binding on the target proteinase: Global stabilization, localized increased structural flexibility, and conserved hydrogen bonding at the active site, *Biochemistry 36*, 5455−5464.
6. Elliott, P. R., Pei, X. Y., Dafforn, T. R., and Lomas, D. A. (2000) Topography of a 2.0 Å structure of α_1-antitrypsin reveals targets for rational drug design to prevent conformational disease, *Protein Sci. 9*, 1274−1281.
7. Im, H., Seo, E. J., and Yu, M. H. (1999) Metastability in the inhibitory mechanism of human α_1-antitrypsin, *J. Biol. Chem. 274*, 11072−11077.
8. Lee, C., Maeng, J. S., Kocher, J. P., Lee, B., and Yu, M. H. (2001) Cavities of α_1-antitrypsin that play structural and functional roles, *Protein Sci. 10*, 1446−1453.
9. Seo, E. J., Im, H., Maeng, J. S., Kim, K. E., and Yu, M. H. (2000) Distribution of the native strain in human α_1-antitrypsin and its association with protease inhibitor function, *J. Biol. Chem. 275*, 16904−16909.
10. Whisstock, J. C., Skinner, R., Carrell, R. W., and Lesk, A. M. (2000) Conformational changes in serpins: I. The native and cleaved conformations of α_1-antitrypsin, *J. Mol. Biol. 295*, 651−665.
11. Irving, J. A., Pike, R. N., Lesk, A. M., and Whisstock, J. C. (2000) Phylogeny of the serpin superfamily: Implications of patterns of amino acid conservation for structure and function, *Genome Res. 10*, 1845−1864.
12. Smith, D. L., Deng, Y., and Zhang, Z. (1997) Probing the non-covalent structure of proteins by amide hydrogen exchange and mass spectrometry, *J. Mass Spectrom. 32*, 135−146.
13. Wales, T. E., and Engen, J. R. (2006) Hydrogen exchange mass spectrometry for the analysis of protein dynamics, *Mass Spectrom. Rev. 25*, 158−170.
14. Kwon, K. S., Kim, J., Shin, H. S., and Yu, M. H. (1994) Single amino acid substitutions of α_1-antitrypsin that confer enhancement in thermal stability, *J. Biol. Chem. 269*, 9627−9631.
15. Laska, M. E. (2001) The effect of dissolved oxygen on recombinant protein degradation in *Escherichia coli*. Ph.D. Thesis, Massachusetts Institure of Technology, Cambridge, MA.
16. Bender, M. L., Begue-Canton, M. L., Blakeley, R. L., Brubacher, L. J., Feder, J., Gunter, C. R., Kezdy, F. J., Killheffer, J. V., Jr., Marshall, T. H., Miller, C. G., Roeske, R. W., and Stoops, J. K. (1966) The determination of the concentration of hydrolytic enzyme solutions: α-Chymotrypsin, trypsin, papain, elastase, subtilisin, and acetylcholinesterase, *J. Am. Chem. Soc. 88*, 5890−5913.
17. Stone, S. R., and Hofsteenge, J. (1986) Kinetics of the inhibition of thrombin by hirudin, *Biochemistry 25*, 4622−4628.
18. Bai, Y., Milne, J. S., Mayne, L., and Englander, S. W. (1993) Primary structure effects on peptide group hydrogen exchange, *Proteins 17*, 75−86.
19. Vriend, G. (1990) WHAT IF: A molecular modeling and drug design program, *J. Mol. Graphics 8*, 52−56, 29.
20. Im, H., Ahn, H. Y., and Yu, M. H. (2000) Bypassing the kinetic trap of serpin protein folding by loop extension, *Protein Sci. 9*, 1497−1502.
21. Bottomley, S. P., Lawrenson, I. D., Tew, D., Dai, W., Whisstock, J. C., and Pike, R. N. (2001) The role of strand 1 of the C β-sheet in the structure and function of α_1-antitrypsin, *Protein Sci. 10*, 2518−2524.
22. Mottonen, J., Strand, A., Symersky, J., Sweet, R. M., Danley, D. E., Geoghegan, K. F., Gerard, R. D., and Goldsmith, E. J. (1992) Structural basis of latency in plasminogen activator inhibitor-1, *Nature 355*, 270−273.
23. Tucker, H. M., Mottonen, J., Goldsmith, E. J., and Gerard, R. D. (1995) Engineering of plasminogen activator inhibitor-1 to reduce the rate of latency transition, *Nat. Struct. Biol. 2*, 442−445.
24. Cho, Y. L., Chae, Y. K., Jung, C. H., Kim, M. J., Na, Y. R., Kim, Y. H., Kang, S. J., and Im, H. (2005) The native metastability and misfolding of serine protease inhibitors, *Protein Pept. Lett. 12*, 477−481.
25. Stein, P. E., and Carrell, R. W. (1995) What do dysfunctional serpins tell us about molecular mobility and disease? *Nat. Struct. Biol. 2*, 96−113.
26. Cabrita, L. D., Dai, W., and Bottomley, S. P. (2004) Different conformational changes within the F-helix occur during serpin folding, polymerization, and proteinase inhibition, *Biochemistry 43*, 9834−9839.
27. Gettins, P. G. (2002) The F-helix of serpins plays an essential, active role in the proteinase inhibition mechanism, *FEBS Lett. 523*, 2−6.
28. Lee, C., Park, S. H., Lee, M. Y., and Yu, M. H. (2000) Regulation of protein function by native metastability, *Proc. Natl. Acad. Sci. U.S.A. 97*, 7727−7731.
29. Gooptu, B., Hazes, B., Chang, W. S., Dafforn, T. R., Carrell, R. W., Read, R. J., and Lomas, D. A. (2000) Inactive conformation of the serpin α_1-antichymotrypsin indicates two-stage insertion of the reactive loop: Implications for inhibitory function and conformational disease, *Proc. Natl. Acad. Sci. U.S.A. 97*, 67−72.
30. Sharp, A. M., Stein, P. E., Pannu, N. S., Carrell, R. W., Berkenpas, M. B., Ginsburg, D., Lawrence, D. A., and Read, R. J. (1999) The active conformation of plasminogen activator inhibitor 1, a target for drugs to control fibrinolysis and cell adhesion, *Structure 7*, 111−118.
31. Richardson, J. S., and Richardson, D. C. (2002) Natural β-sheet proteins use negative design to avoid edge-to-edge aggregation, *Proc. Natl. Acad. Sci. U.S.A. 99*, 2754−2759.
32. Kumar, S., Ma, B., Tsai, C. J., Sinha, N., and Nussinov, R. (2000) Folding and binding cascades: Dynamic landscapes and population shifts, *Protein Sci. 9*, 10−19.
33. Luque, I., Leavitt, S. A., and Freire, E. (2002) The linkage between protein folding and functional cooperativity: Two sides of the same coin? *Annu. Rev. Biophys. Biomol. Struct. 31*, 235−256.
34. Wintrode, P. L., and Arnold, F. H. (2000) Temperature adaptation of enzymes: Lessons from laboratory evolution, *Adv. Protein Chem. 55*, 161−225.
35. Roberts, T. H., Hejgaard, J., Saunders, N. F., Cavicchioli, R., and Curmi, P. M. (2004) Serpins in unicellular eukarya, archaea, and bacteria: Sequence analysis and evolution, *J. Mol. Evol. 59*, 437−447.
36. Lomas, D. A., Evans, D. L., Upton, C., McFadden, G., and Carrell, R. W. (1993) Inhibition of plasmin, urokinase, tissue plasminogen activator, and C1S by a myxoma virus serine proteinase inhibitor, *J. Biol. Chem. 268*, 516−521.
37. Simonovic, M., Gettins, P. G. W., and Volz, K. (2000) Crystal structure of viral serpin crmA provides insights into its mechanism of cysteine proteinase inhibition, *Protein Sci. 9*, 1423−1427.
38. Koradi, R., Billeter, M., and Wuthrich, K. (1996) MOLMOL: A program for display and analysis of macromolecular structures, *J. Mol. Graphics 14*, 51−55, 29−32.
39. DeLano Scientific (2002) The PyMOL Molecular Graphic System, San Caros, CA, http://www.pymol.org.

BI060431F